Quantitative Microbiology 2, 249–270, 2000

Mathematical Modeling of Ultraviolet Germicidal Irradiation for Air Disinfection

W. J. KOWALSKI*
Department of Architectural Engineering, The Pennsylvania State University, Engineering Unit A, University Park, PA 16802, USA
**Corresponding author: e-mail: drKowalski@psu.edu*

W. P. BAHNFLETH
Department of Architectural Engineering, The Pennsylvania State University, Engineering Unit A, University Park, PA 16802, USA

D. L. WITHAM
Ultraviolet Devices, Inc., 28220 Industry Drive, Valencia, CA 91355, USA

B. F. SEVERIN
M.B.I. International, P.O. Box 27609, 3900 Collins Road, Lansing, MI 48909, USA

T. S. WHITTAM
Department of Microbiology and Molecular Genetics, Michigan State University, East Lansing, MI 48824, USA

Received January 12, 2001; Accepted October 4, 2001

Abstract. A comprehensive treatment of the mathematical basis for modeling the disinfection process for air using ultraviolet germicidal irradiation (UVGI). A complete mathematical description of the survival curve is developed that incorporates both a two stage inactivation curve and a shoulder. A methodology for the evaluation of the three-dimensional intensity fields around UV lamps and within reflective enclosures is summarized that will enable determination of the UV dose absorbed by aerosolized microbes. The results of past UVGI studies on airborne pathogens are tabulated. The airborne rate constant for *Bacillus subtilis* is confirmed based on results of an independent test. A re-evaluation of data from several previous studies demonstrates the application of the shoulder and two-stage models. The methods presented here will enable accurate interpretation of experimental results involving aerosolized microorganisms exposed to UVGI and associated relative humidity effects

Key words: UVGI, UV air disinfection, surface disinfection, survival curve, decay curve

1. Introduction

Ultraviolet radiation in the range 225–302 nm is lethal to microorganisms and is referred to as ultraviolet germicidal irradiation (UVGI). Water and surface disinfection with UVGI are proven and reliable technologies, but airstream disinfection systems have had varying and unpredictable performance in applications. In spite of the widespread use of UVGI today for air disinfection and microbial growth control, design information about the effects of UVGI on airborne pathogens lacks the detail necessary to guarantee predictable

performance. In addition, few airborne rate constants are known with certainty due to the inherent difficulties of setting up an experiment and accurately interpreting test results.

The methods described here will facilitate the experimental design and accurate interpretation of aerosol studies on the inactivation of airborne pathogens with UVGI, as well as assist the design of UVGI systems for specific applications. Two distinct components make up the complete model—a model of microbial decay under UVGI exposure that depends on the microorganism, and a model of the UV dose resulting from the UVGI system or test apparatus.

2. Modeling Microbial Decay

The classical exponential decay model treats microbial survival under the influence of any biocidal factor (Chick, 1908). The refinements presented here, the two-stage model and the shoulder model, extend its applicability. One alternative model, the multi-hit target model is also capable of accounting for the shoulder and two stages of inactivation. The latter has been adequately addressed elsewhere and is summarized here for comparison purposes at the end of this section.

Microorganisms exposed to UVGI experience an exponential decrease in population similar to other methods of disinfection such as heating, ozonation, and exposure to ionizing radiation (Koch, 1995; Mitscherlich and Marth, 1984). The single stage exponential decay equation for microbes exposed to UV irradiation is as follows:

$$S = \mathrm{e}^{-kIt} \tag{1}$$

where $S =$ surviving fraction of initial microbial population, $k =$ standard rate constant ($\mathrm{cm}^2/\mu\mathrm{J}$), $I =$ UV intensity ($\mu\mathrm{W}/\mathrm{cm}^2$), $t =$ time of exposure (seconds) and where $1\ \mu\mathrm{J} = 1\ \mu\mathrm{W\text{-}s}$.

The rate constant defines the sensitivity of a microorganism to UV exposure and is unique to each microbial species. Most published test results provide an overall rate constant that applies only at the test intensity. The standard rate constant k in equation (1) is the equivalent rate constant at an intensity of $1\ \mu\mathrm{W}/\mathrm{cm}^2$ and is found by dividing any measured rate constant by the test intensity. The standard rate constant, therefore, is independent of intensity.

The intensity in equation (1) can be considered to represent either the irradiance on a flat surface or the fluence rate through the outer surface of a solid (i.e. a spherical microbe). If the average intensity is constant, or can be calculated, then the standard rate constant can be computed as

$$k = \frac{-\ln S}{It}. \tag{2}$$

The value of the rate constant depends on whether the intensity is defined as irradiance or fluence rate, and can also depend on how it is measured. This matter is addressed in the section on UV dose. Table 1 lists some 30 pathogens and rate constants determined in

Table 1. UVGI rate constants for respiratory pathogens.

Microorganism	Type	Reference	Test medium Air/Plt/Wtr	k = Standard rate constant ($cm^2/\mu J$)
Adenovirus	Virus	Jensen, 1964	Air	0.000546
		Rainbow, 1973	Plates	0.000047
Vaccinia	Virus	Jensen, 1964	Air	0.001528
		Galasso, 1965	Plates	0.001542
Coxsackievirus	Virus	Jensen, 1964	Air	0.001108
		Hill, 1970 (B-1)	Water	0.000159
		Hill, 1970 (A-9)	Water	0.000202
Influenza A	Virus	Jensen, 1964	Air	0.001187
Echovirus	Virus	Hill, 1970	Water	0.000217
Reovirus Type 1	Virus	Hill, 1970	Water	0.000132
Staphylococcus aureus	Gram+ Bacteria	Sharp, 1939	Plates	0.000886
		Sharp, 1940	Air	0.003476
		Gates, 1929	Plates	0.001184
		Abshire, 1981	Plates	0.000419
		Luckiesh, 1946	Air	0.009602
Streptococcus pyogenes	Gram+ Bacteria	Lidwell, 1950	Plates	0.006161
		Mitscherlich, 1984	Air	0.001066
Mycobacterium tuberculosis	Mycobacteria	David, 1973	Air	0.000987
		Riley, 1976	Air	0.004721
		Collins, 1971	Air	0.002132
Mycobacterium kansasii	Mycobacteria	David, 1973	Air	0.000364
Mycobacterium avium-intra.	Mycobacteria	David, 1973	Air	0.000406
E. coli (reference only)	Gram− Bacteria	Sharp, 1939	Plates	0.000927
		Sharp, 1940	Air	0.003759
Corynebacterium diptheriae	Gram+ Bacteria	Sharp, 1939	Plates	0.000701
Moraxella-Acinetobacter	Gram− Bacteria	Keller, 1982	Water	0.0000021
Haemophilus influenzae	Gram− Bacteria	Mongold, 1992	Plates	0.000599
Pseudomonas aeruginosa	Gram− Bacteria	Collins, 1971	Air	0.002375
		Abshire, 1981	Water	0.000640
		Sharp, 1940	Air	0.005721
		Antopol, 1979	Water	0.000419
Legionella pneumophila	Gram− Bacteria	Gilpin, 1984	Water	0.002047
		Antopol, 1979	Water	0.002503
Serratia marcescens	Gram− Bacteria	Collins, 1971	Air	0.002208
		Antopol, 1979	Water	0.001047
		Riley, 1972	Air	0.049900
		Sharp, 1940	Air	0.004449
		Sharp, 1939	Air	0.001047
		Rentschler, 1941	Air	0.001225
Coxiella burnetti	Rickettsiae	Little, 1980	Water	0.001535
Bacillus anthracis	Mixed spores	Sharp, 1939	Plates	0.000509
Bacillus anthracis	Bacterial spore	Knudson, 1986	Plates	0.000031
Cryptococcus neoformans	Fungal spore	Wang, 1994	Plates	0.000102
Fusarium oxysporum	Fungal spore	Asthana, 1992	Plates	0.000112
Fusarium solani	Fungal spore	Asthana, 1992	Plates	0.0000706
Penicillium italicum	Fungal spore	Asthana, 1992	Plates	0.0001259
Penicillium digitatum	Fungal spore	Asthana, 1992	Plates	0.0000718
Rhizopus nigricans	Fungal spore	Luckiesh, 1946	Air	0.0000861

(*continued*)

Table 1. (*continued*)

Microorganism	Type	Reference	Test medium Air/Plt/Wtr	k = Standard rate constant ($cm^2/\mu J$)
Cladosporium herbarum	Fungal spore	Luckiesh, 1946	Air	0.0000370
Scopulariopsis brevicaulis	Fungal spore	Luckiesh, 1946	Air	0.0000344
Mucor mucedo	Fungal spore	Luckiesh, 1946	Air	0.0000399
Penicillium chrysogenum	Fungal spore	Luckiesh, 1946	Air	0.0000434
Aspergillus amstelodami	Fungal spore	Luckiesh, 1946	Air	0.0000344

various media. The wide variation in rate constants predicted reflects the differences in media, the test arrangements, and the methods of measuring the intensity. In general, aerosol studies yield moderately higher rate constants than plate studies. This could be expected since microbes tumbling in the air will receive exposure all around, while microbes on plates receive exposure in one plane only.

Two-stage survival curves. In general, a small fraction of any microbial population is resistant to UVGI or other bactericidal factors (Cerf, 1977; Fujikawa and Itoh, 1996). Typically, over 99% of the microbial population will succumb to initial exposure but a remaining fraction will survive, sometimes for prolonged periods (Smerage and Teixeira, 1993; Qualls and Johnson, 1983). This effect may be due to clumping (Moats *et al*., 1971; Davidovich and Kishchenko, 1991), dormancy (Koch, 1995), or other factors.

The two-stage survival curve can be represented mathematically as the summed response of two separate microbial populations that have respective rate constants k_1 and k_2. If we define f as the resistant fraction of the total initial population with rate constant k_2, then $(1-f)$ is the fraction with rate constant k_1. The total survival curve is therefore the sum of the rapid decay curve (the vulnerable majority) and the slow decay curve (the resistant minority).

$$S(t) = (1-f)e^{-k_1 It} + f e^{-k_2 It} \tag{3}$$

where k_1 = rate constant for fast decay population ($cm^2/\mu J$), k_2 = rate constant for resistant population ($cm^2/\mu J$), f = resistant fraction.

Figure 1 shows data for *Streptococcus pyogenes* that displays two-stage behavior. The resistant fraction of most microbial populations may be about 0.01–1% but some studies suggest it can be a large fraction for certain species (Riley and Kaufman, 1972; Gates, 1929).

Values of the two-stage rate constants are summarized in Table 2 for the few microbes for which second stage data has been published. These parameters represent a re-interpretation of the original published results by the indicated researchers and in all cases an improved curve-fit resulted. The two-stage rate constants k_1 and k_2 listed in

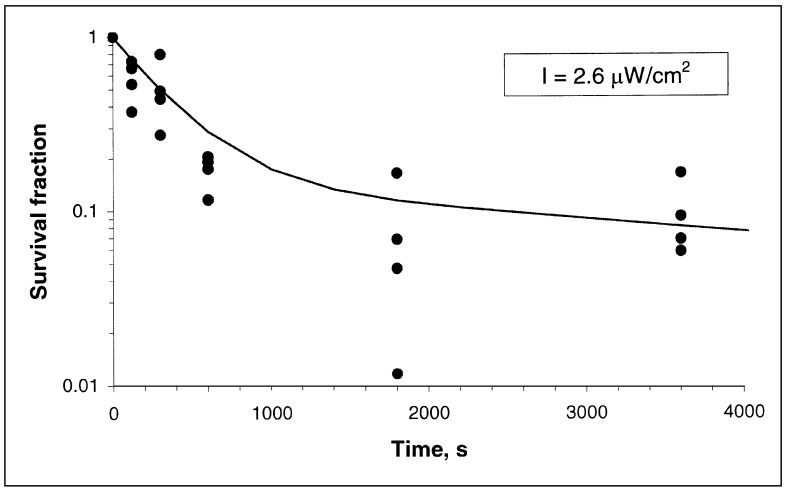

Figure 1. Survival curve of *Streptococcus pyogenes* showing two stages, based on data from Lidwell (1950).

Table 2. Two stage parameters (based on re-evaluation of original data).

Airborne microorganism	Reference	k standard ($cm^2/\mu J$)	Two stage curve			
			k_1 ($cm^2/\mu J$)	Pop. (f)	k_2 ($cm^2/\mu J$)	Pop. ($1-f$)
Adenovirus Type 2	Rainbow, 1973	0.000047	0.00005	0.99986	0.00778	0.00014
Coxsackievirus B-1	Hill, 1970	0.000202	0.000248	0.9807	8.81E-05	0.0193
Coxsackievirus A-9	Hill, 1970	0.000159	0.00016	0.7378	0.000125	0.2622
Staphylococcus aureus	Sharp, 1939	0.000886	0.01702	0.914	0.0091	0.086
Streptococcus pyogenes	Lidwell, 1950	0.000616	0.00287	0.8516	0.000167	0.1484
E. coli (Reference only)	Sharp, 1939	0.000927	0.008098	0.9174	0.003947	0.0826
Serratia marcescens	Riley, 1972	0.049900	0.0757	0.712	0.0292	0.288
Bacillus anthracis spores	Knudson, 1986	0.000031	0.000042	0.9984	0.000006	0.0016

Table 2 are overall rate constants that apply only at the intensity shown, which is the UV irradiation measured or given in the original test.

The shoulder. The initiation of exponential decay in response to UVGI exposure, or any other biocidal factor, is often delayed for a brief period of time (Cerf, 1977; Munakata *et al*., 1991; Pruitt and Kamau, 1993). Figure 2 shows the survival curve for *Staphylococcus aureus*, where a shoulder is evident from the fact that the regression line intercepts the y axis above unity. Shoulder curves typically start out horizontally before developing full exponential decay slope.

As shown in Figure 3, the initial part of the decay curve has zero slope at time $t = 0$ and exponential decay is not fully manifested until time t_d. The intersection of the horizontal line

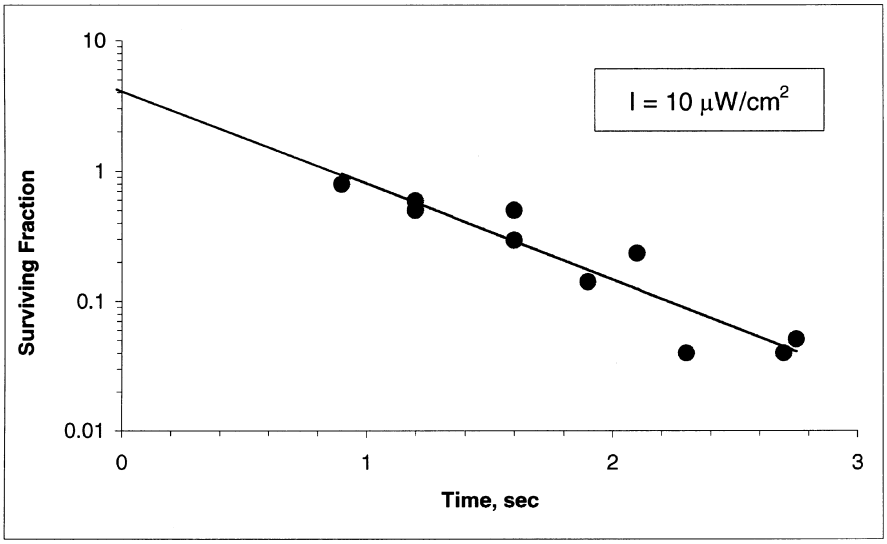

Figure 2. Survival curve of *Staphylococcus aureus* showing evidence of shoulder (Sharp, 1939).

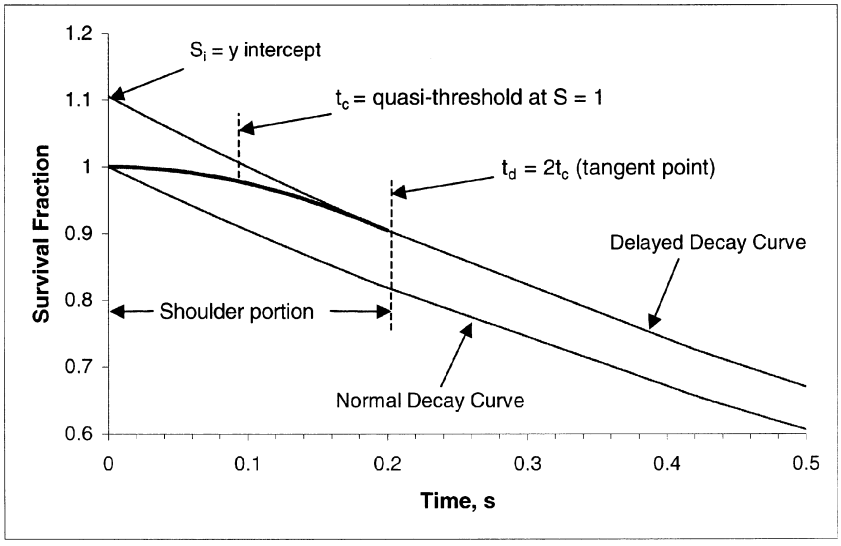

Figure 3. Development of shoulder curve, showing the effect of the time delay t_c and relation to the tangent point d.

$S = 1$ (100% Survival) at t_c with the extension of the decay curve is known as the "quasi-threshold" in radiation biology (Casarett, 1968). The point t_d is tangent to both curves.

The lag in response to the stimulus implies that either a threshold dose is necessary before measurable effects occur or that repair mechanisms actively deal with low-level damage (Casarett, 1968). The effect is species and intensity dependent. In many cases it can be neglected. However, for some species and sometimes for low intensity exposure, the shoulder can be significant and prolonged.

Recovery due to growth during irradiation is assumed negligible and to be encompassed by the model—this should be at least partly true if the parameters are based on a broad range of empirical data. Recovery of spores, although not well understood, is recognized as a process associated with germination (Russell, 1982). The recovery of spores is, therefore, a self-limiting factor since a germinated spore invariably becomes less resistant to UVGI irradiation (Harm, 1980).

An exponential decay curve with a shoulder will have an intercept greater than unity when the first stage rate constant is extrapolated to the y-axis. It is naturally assumed that a shoulder exhibited in the data is statistically significant and not an artifact of measurement uncertainty. Relative to a decay curve that intercepts at unity, the shouldered curve is shifted ahead by a time interval equal to t_c, the quasi-threshold. The equation for the delayed single stage survival curve, when $t \geq t_d$ is:

$$\ln S(t) = -kI(t - t_c). \tag{4}$$

The shoulder occurs during the time interval $0 < t < t_d$. It is apparent that the shoulder portion is a non-linear function of $\ln S$ (see Figure 2). Insufficient data exist to precisely define the form of the relationship, but $\ln S$ cannot be simpler than a polynomial function of second order. The error resulting from this assumed mathematical relationship will be small as long as it provides a smooth transition between the horizontal and the delayed decay curve.

Assuming a second order polynomial relationship between the dose (intensity times time) and $\ln S$, we have:

$$\ln S(t) = -p(It)^2 \tag{5}$$

where $0 < t < t_d$, $p =$ a constant.

The constant p can be evaluated by requiring continuity through the first derivative between equations (4) and (5) at the tangent point $t = t_d$. For any constant intensity I, the slope of the exponential portion of the survival curve may be obtained by straightforward time differentiation of the right hand side of equation (4):

$$\frac{d}{dt}(\ln S) = -kI \tag{6}$$

Similarly, the slope of the shoulder curve is obtained by differentiation of the right hand side of equation (5):

$$\frac{\mathrm{d}}{\mathrm{d}t}(\ln S) = -2pI^2t \tag{7}$$

The constant p is determined by equating (6) and (7) at time t_d:

$$p = \frac{k}{2It_\mathrm{d}} \tag{8}$$

Substitution of this expression for p into equation (5) and equating (6) and (7) at $t = t_\mathrm{d}$ yields the relation:

$$t_\mathrm{d} = 2t_\mathrm{c} \tag{9}$$

Equation (9) is, in fact, a version of the result Appolonius of Perga arrived at in the 3rd century BC through lengthy geometry for the special case of ellipses, which are also described by second order polynomials (Elmer, 1989). The term p is now discarded, after substituting for equations (8) and (9), and equation (5) can be written in the form:

$$\ln S = -\frac{kI}{4t_\mathrm{c}}t^2 \tag{10}$$

In general, any data set describing single stage microbial decay can be easily fit to a single stage exponential decay curve. Normally, the y-intercept is fixed at $S = 1$ when fitting data to a curve. If a shoulder is suspected, the constraint on the y-intercept should be removed and the coefficient of the exponential will then have some value greater than 1. This assumes, of course, that the shoulder is real and not a result of measurement uncertainty.

The term S_i, denotes the y-intercept of the shifted exponential portion of a survival curve with a shoulder, as shown in Figure 4. If S_i is known, the value of t_c can be determined by evaluating equation (4) at $t = 0$:

$$t_\mathrm{c} = \frac{\ln(S_\mathrm{i})}{kI} \tag{11}$$

Note that this mathematical treatment of the shoulder requires transcending the dose term It since this must be separated into components. The dose may define a point on the shoulder but the intensity defines the shoulder itself. That is, the threshold t_c is a function of the intensity only, not the dose. Furthermore, in two stage curves there is a separate shoulder for both stages, although the contribution due to the second stage (the resistant fraction) is typically small.

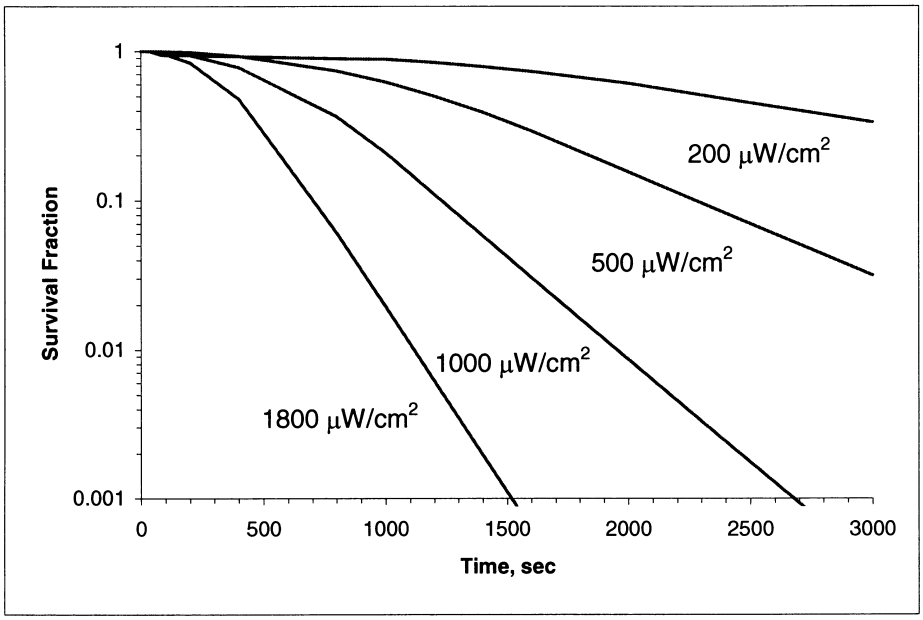

Figure 4. Illustration of generic shoulder model response to intensity, based on data for *Aspergillus niger* from UVDI (2000).

The complete single stage survival curve can then be defined as the piecewise continuous function:

$$\ln S(t) = \begin{cases} -\dfrac{kI}{4t_c}\, t^2, & t \le 2t_c \\ -kI(t - t_c), & t \ge 2t_c \end{cases} \tag{12}$$

The time delay (the threshold t_c) may approach zero at high intensities and it may be infinitely long for low intensities. For $t_c = 0$ equation (12) reduces to equation (1).

No studies exist that define the relationship between the threshold and the intensity but data from Riley and Kaufman (1972) suggests that a linear relation exists between intensity and the logarithm of the y-intercept S_i. A theoretical basis can be found for the same relationship in the Arrhenius rate equation, which describes the influence of temperature or radiation on process rates as being that of simple exponential decay (Rohsenow and Hartnett, 1973). Assuming, therefore, that the threshold t_c is an exponential function of the intensity I we can write:

$$t_c = A\mathrm{e}^{-BI} \tag{13}$$

where $A =$ a constant defining the intercept at $I = 0$, $B =$ a constant defining the slope of the plotted line of $\ln(t_c)$ vs. I.

Given any two sets of data for t_c and I, equation (13) can be used to determine the values of A and B. Prediction of t_c for any arbitrary value of intensity I then becomes possible. Figure 4 shows hypothetical survival curves of spores subject to various intensities.

The complete equation can be defined by combining equation (3) and equation (12), where a shoulder is considered to be present in both stages:

$$S(t) = f e^{-k_1 I t'} + (1 - f) e^{-k_2 I t'} \tag{14}$$

where

$$t' = \begin{cases} \dfrac{t^2}{4t_c}, & t \le 2t_c \\ (t - t_c), & t \ge 2t_c \end{cases}$$

Parameters defining the shoulder characteristics of various microbes are summarized in Table 3. These were obtained by re-interpretation of the original published results by the indicated researchers and in all cases an improved curve-fit resulted. The parameters 'A' and 'B', the threshold t_c, and the intensity I cannot be established due to the paucity of data in the literature for different intensities.

A few cases were found in the literature where the first stage intercept proved to be less than 1, which is probably due to experimental error and limited data sets. In all cases when shoulder parameters are evaluated, an error analysis should be performed to verify that the results defining the shoulder and second stage are meaningful.

The multi-hit target model

Alternate mathematical models have been proposed to account for the shoulder including the multi-hit model or multi-target model, recovery models, split-dose recovery models,

Table 3. Shoulder parameters for classical and multi-hit models.

Airborne microorganism (see Table 1 for References)	Reference	k standard ($cm^2/\mu J$)	Classical model			Multi-hit model (n)
			Intensity ($\mu W/cm^2$)	Intercept (S_i)	Threshold (t_c)	
Reovirus Type 1	Hill, 1970	0.000132	1160	1.7237	3.1202	1.29
Staphylococcus aureus	Sharp, 1939	0.000886	10	4.4246	87.38	4.92
	Gates, 1929	0.001184	110	1.225	1.8432	1.69
Mycobacterium tuberculosis	David, 1973	0.000987	400	2.6336	4.176	2.34
	Riley, 1961	0.004720	85	1.7863	3	1.83
Mycobacterium kansasii	David, 1973	0.000364	400	6	4.254	6.11
Mycobacterium avium-intra.	David, 1973	0.000406	400	5.62	9.227	5.97
Haemophilus influenzae	Mongold, 1992	0.000599	50	1.0902	2.5703	1.18
Pseudomonas aeruginosa	Abshire, 1981	0.000640	100	1.3858	9.6818	1.77
Legionella pneumophila	Antopol, 1979	0.002503	50	1.288	96.69	1.67
Serratia marcescens	Rentschler, 1941	0.001225	1	2.0824	190.5	1.71
Bacillus anthracis (mixed)	Sharp, 1939	0.000509	1	2.0806	109.8	2.63
Bacillus anthracis spores	Knudson, 1986	0.000031	90	1.009	215	2.60

and empirical models (Russell, 1982; Harm, 1980; Casarett, 1968). The use of the multi-hit target model, for example, to determine shoulder characteristics is similar in form to the methods for the classical model (Anellis *et al*., 1965), and is addressed here for comparison purposes.

The multi target model (Severin *et al*., 1983) can be written as follows:

$$S(t) = 1 - \left(1 - e^{-kIt}\right)^n \tag{15}$$

The parameter n represents the number of discrete critical sites that must be hit to inactivate the microorganism, and is unique for each species.

In equation (15) the number of targets n must be unique to each population fraction in a two stage curve, since these behave as though they were independent. Therefore, by analogy to equation (14) we can write the complete two stage equation for the multi-hit model as follows:

$$S(t) = (1-f)\left[1 - (1 - e^{-k_1 It})^{n_1}\right] + f\left[1 - (1 - e^{-k_2 It})^{n_2}\right] \tag{16}$$

In equation (16), n_1 represents the number of targets for the species in population 1, the fast decay population, while n_2 represents the number of targets in the resistant fraction. Figure 5 shows a comparison of shoulder curves generated by the classical model and the multi-hit model compared against test data on *Staphylococcus aureus* irradiated on petri dishes. The curves do not exactly coincide, but the question of which model is a more

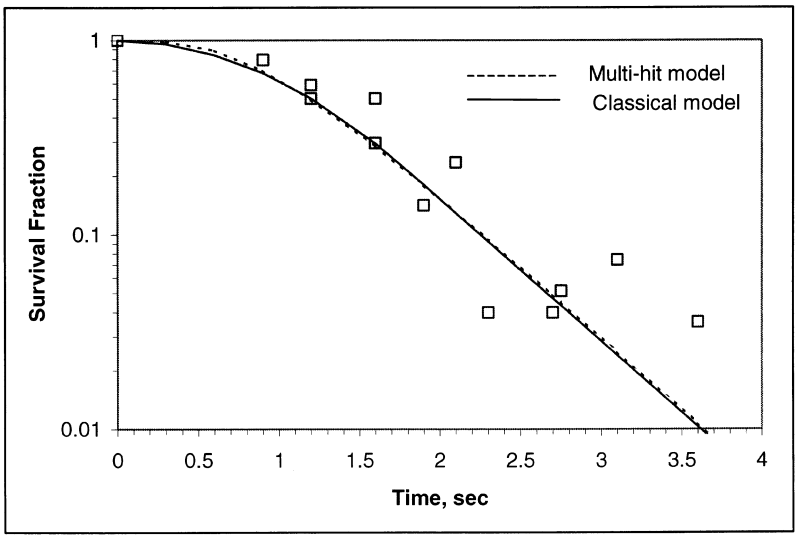

Figure 5. Comparison of classical shoulder model and multi-hit model with data for exposed plates of *Staphylococcus aureus*. Based on data from Sharp (1939) at an estimated test intensity of 1900 $\mu W/cm^2$.

accurate predictor is indeterminate due to experimental error. It remains for future research to determine which model is a more accurate predictor of shoulder curves. Either model should suffice for basic analysis and design purposes.

Table 3 includes the value of n, the number of targets, for the multi-hit model which have been derived from the original test data. These can be used to generate a single stage shoulder curve similar to the one for the listed shoulder parameters. In all cases the multi-hit model curve does not exactly coincide with the one produced by the classical model, yet the error is quite small.

3. Modeling the UV Dose

Two approaches can be taken to define the complete three-dimensional (3D) intensity field in any experimental apparatus involving airflow—measurement and calculation. Photosensors can provide a profile of the field but they have inherent problems in the near field (Severin and Roessler, 1998) and have difficulties when used inside reflective enclosures. The question of whether photosensors can be used to measure the fluence rate that an airborne microbe actually experiences is an unresolved one. Recent advances in the use of spherical actinometry (Rahn *et al*., 1999) may provide more realistic results since these sensors more closely resemble spherical microbes.

The problems of photosensing and data interpretation can be avoided through analytical determination of the 3D intensity field. The use of radiation view factors to define the 3D intensity field for both the lamp and internal reflective surfaces has been detailed by Kowalski and Bahnfleth (2000) and is summarized here.

Various models of the intensity field due to UV lamps have been proposed in the past, including point source, line source, integrated line source, and other models (Jacob and Dranoff, 1970; Qualls and Johnson, 1983; Beggs *et al*., 2000). The model used here is based on thermal radiation view factors (Modest, 1993), which define the amount of diffuse radiation transmitted from one surface to another.

Figure 6 illustrates a lamp modeled as a cylinder where the planar area at which the UV intensity is to be determined is perpendicular to the axis and is at the edge of the cylinder. The fraction of radiative intensity that leaves the cylindrical body and arrives at a differential area (Modest, 1993) is:

$$F = \frac{L}{\pi H}\left[\begin{array}{c} \dfrac{1}{L}\mathrm{ATAN}\left(\dfrac{L}{\sqrt{H^2-1}}\right) - \mathrm{ATAN}(M) \\ + \dfrac{X-2H}{\sqrt{XY}}\mathrm{ATAN}\left(M\sqrt{\dfrac{X}{Y}}\right) \end{array}\right] \tag{17}$$

The parameters in equation (17) are defined as follows:

$$H = x/r \qquad L = l/r \qquad X = (1+H)^2 + L^2$$

$$Y = (1-H)^2 + L^2 \qquad M = \sqrt{\frac{H-1}{H+1}}$$

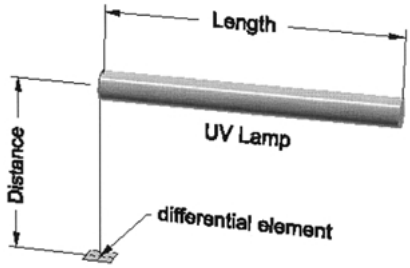

Figure 6. View factor geometry for computing the intensity at a point some distance from the axis of a lamp modeled as a radiating cylinder.

where l = length of the lamp segment (arclength, cm), x = distance from the lamp (cm), r = radius of the lamp (cm).

This equation applies to a differential element located at the edge of the lamp segment. In order to compute the view factor at any point along a lamp it must be divided into two segments. Equation (17) can be used to compute the intensity at any point beyond the ends of the lamp by applying it twice—once to compute the view factor for an imaginary lamp of the total length (distance between some point and the far end of the lamp) and then subtracting the view factor of the non-existent portion, or ghost portion. This method, known as view factor algebra, is detailed in Kowalski and Bahnfleth (2000) and elsewhere (Modest, 1993).

Implicit in the use of this view factor is the spherical microbe assumption, or the assumption that microbes are spherical. In the view factor model, the cross-sectional area of a sphere is a flat disc that remains perpendicular to a line passing through the lamp axis, as shown in Figure 7. A source of error in this assumption is due to the fact that light rays coming from other parts of the lamp, as illustrated in the figure, are not always perpendicular to the disc surface. Analysis by the authors using a view factor model in

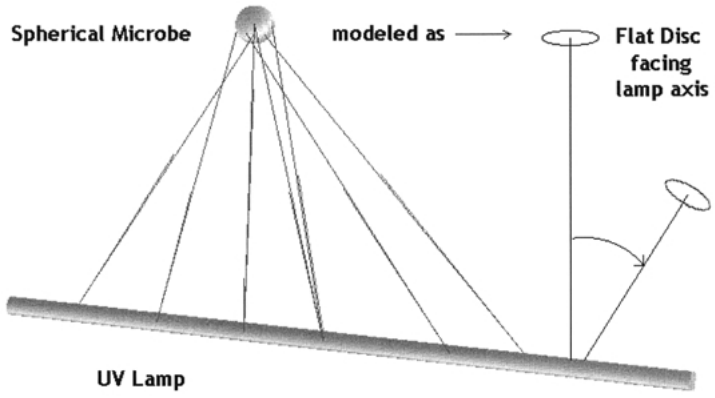

Figure 7. Modeling of a spherical microbe as a flat disc (the cross-section of a sphere) that always faces the lamp axis.

which the intensity has been corrected for the cosines of the angles from non-perpendicular rays has established that this difference is quite small and can be neglected in most cases. This is due to the fact that when the disc element is close to the lamp surface the nearest sections of the lamp dominate the intensity field, while at large distances the cosines become small.

The intensity field as a function of distance from the lamp axis is simply the product of the surface intensity and the view factor, where the surface intensity is computed by dividing the UV power output by the surface area of the lamp:

$$I = \frac{E_{\text{uv}}}{2\pi rl} F_{\text{total}} \tag{18}$$

where $E_{\text{uv}} =$ UV power output of lamp, μW.

Figure 8 illustrates photosensor data on a UV lamp compared against the predictions of the view factor model and a line source model. The line source model used in this figure is based on Beggs *et al*. (2000) and appears to underpredict the intensity field. Data from a number of other lamp models were reviewed and in all cases good agreement with the view factor model was obtained while other line source models typically deviate from perfect agreement with photosensor data (Kowalski and Bahnfleth, 2000).

UV lamps have published ratings based on measurements taken at 1 m from the midpoint of the lamp axis (IES, 1981). The rated intensity for any tubular lamp can be computed by using equation (17) with two equal lamp segments. Figure 9 shows the view

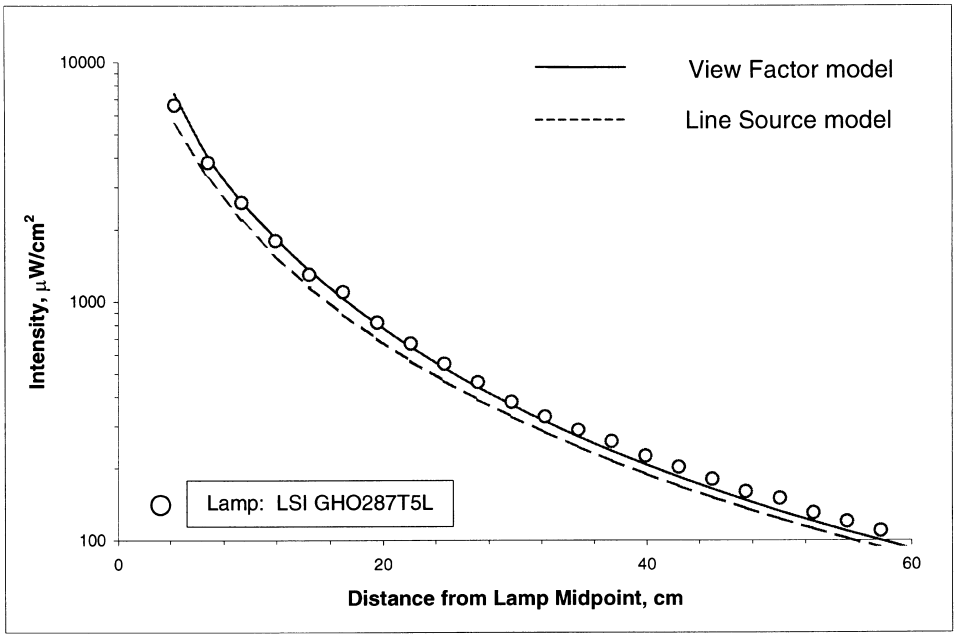

Figure 8. Comparison of view factor model and line source model predictions at the midpoint of typical UV lamps with photosensor data.

factor model predictions of lamp ratings for almost one hundred commercially available UV lamps. Shown also are the predictions for a line source model, based on Beggs *et al*. (2000), in which it can be observed that good agreement is obtained for small lamps but that deviations progressively occur for larger lamps.

Although the line source models tend to underpredict the intensity field, it should be noted that water-based disinfection with UVGI depends more heavily on near-field absorbance, and for such applications these models are capable of providing adequate results (Suidan and Severin, 1986). Air disinfection involves much larger distances and dimensions than water disinfection and so the accuracy of the model at these distances becomes more of a factor.

UV intensity field due to enclosure reflectivity. In a rectangular duct, each of the four walls will reflect a fraction of the incident intensity it experiences at the surface. If the UV reflectivity is 75%, then 75% of the UV intensity that occurs at the surface (due to the UV lamp) will be reflected back into the enclosed space. The intensity at each surface is computed using equation (17), after which the intensity field due to the radiating flat rectangular surface can be computed by the following view factor equation (Modest, 1993):

$$F_{\mathrm{h}} = \frac{1}{2\pi}\left[\begin{array}{l} \dfrac{X}{\sqrt{1+X^2}}\mathrm{ATAN}\left(\dfrac{Y}{\sqrt{1+X^2}}\right) \\ +\dfrac{Y}{\sqrt{1+Y^2}}\mathrm{ATAN}\left(\dfrac{X}{1+Y^2}\right) \end{array}\right] \tag{19}$$

where $X = \mathrm{Height}/x$, $Y = \mathrm{Length}/x$, $x =$ perpendicular distance to the wall.

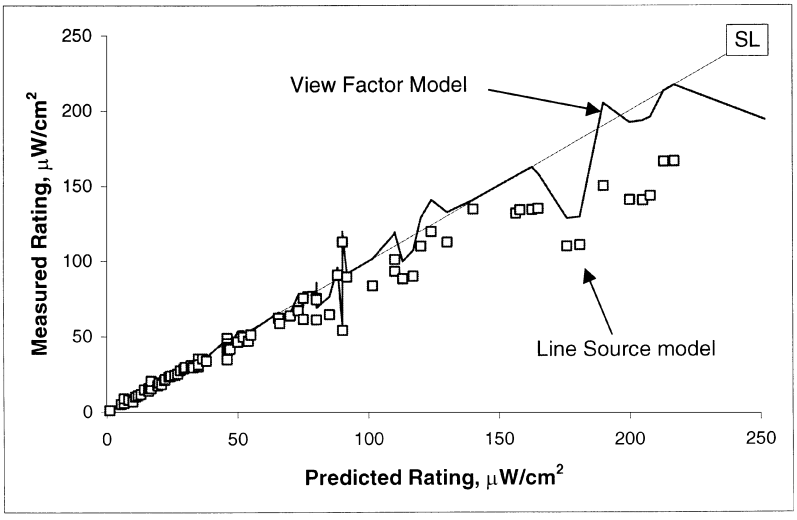

Figure 9. Comparison of measured UV lamp ratings with predictions of the view factor model and a line source model (Beggs *et al*., 2000). The straight line (SL) represents perfect predictions.

This view factor is consistent with the previously stated spherical microbe assumption in that equation (19) is applied to all four walls as if the microbe faced each one individually. The intensity field due to each surface is then summed to obtain the total reflected intensity field. The error due to the fact that some portions of the rectangular surface are not perpendicular to the flat disc element that represents the spherical microbe is negligible for the same reasons discussed previously. In addition, the distances to the walls are, in general greater, and the surface intensities lower, rendering the error still more negligible.

Subsequent reflections, called inter-reflections, can be accounted for with more sophisticated computational methods (Kowalski and Bahnfleth, 2000; Kowalski, 2001), but equation (19) may suffice as a reasonable first order approximation if the material has low reflectivity.

Rate constant determination. Previously, no analytical method existed to enable researchers to accurately evaluate the intensity field and assess the dose received by airborne microbes in experimental setups. As a result, airborne rate constants could not easily be determined. In some airborne experiments the airstream was confined to an area of known intensity by directing airflow through a narrow slot (Riley and Kaufman, 1972).

Given the methods and analytical tools described above, airborne rate constants can now be determined with improved accuracy. As mentioned previously, rate constants depend on the test apparatus and measurement methods and so are relative to the experiment from which they come. The analytical methods presented here enable easy resolution of the intensity field and can readily predict rate constants, but with the caveat that these rate constants are, in turn, dependent on these methods. That is to say, an airborne rate constant determined with the present methods can be used for predictive purposes, but only if these methods are also used for the predictions. Otherwise, what certainty there is in the prediction would be diminished.

4. Air Mixing Effects

In long ducts the velocity profile of a laminar airstream will approach a parabolic shape, with the velocity higher towards the center. However, fully developed laminar velocity profiles are unlikely to be achieved in laboratory or real-world installations. The design velocity of a typical UVGI system is about 2.54 m/s (500 fpm), producing a Reynolds number of approximately 150,000. Turbulent mixing is therefore more likely to be the norm. Even laminar flow involves mixing by diffusion and so actual operating conditions will lie somewhere between complete mixing and the idealized condition of completely unmixed flow. Real world conditions tend to approach those of complete mixing, and such was shown by Severin *et al*. (1984) for water-based systems.

These bounding conditions, complete mixing and unmixed flow, assume a flat velocity profile. Rate constants due to the latter are computed using the average intensity. The total survival, for each stage if there are two stages in the survival curve, is as follows:

$$S = \mathrm{e}^{-kI_{\mathrm{avg}}t} \tag{20}$$

where $I_{\mathrm{avg}} =$ average intensity in the irradiation chamber ($\mu\mathrm{W/cm^2}$).

The average intensity can be computed for any irradiation chamber using equations (17) and (19) with a 3D matrix of sufficient resolution. A computer model developed by the authors uses a matrix of $50 \times 50 \times 100$ with satisfactory results.

If the airflow through a UVGI chamber followed perfectly parallel streamlines without mixing then each streamline will produce a unique dose that depends on the distance from the lamp. The survival rate in this case must be calculated for each streamline segment and summed or 'integrated' to obtain the net survival. The survival S_i for each streamline segment is computed by equation (20) and the total survival would be the sum of all streamline segments as follows:

$$S = \sum_{j=1}^{l} \sum_{i=1}^{m} \sum_{k=1}^{n} e^{-kI_{ijk}t} \tag{21}$$

where I_{ijk} = Intensity at point ijk, i = a point defining the x coordinate (width), j = a point defining the y coordinate (height), k = a point defining the z coordinate (length), t = exposure time for each segment defined by point ijk.

The exposure time is constant for each streamline segment. The population is assumed to be equally divided among all streamlines in the flat velocity profile. In the event the velocity profile is known and is not flat, the exposure time in equation (21) can be indexed to account for the actual velocities.

Equation (21) permits the development of a contour map of the 'kill zones' of the unmixed condition for any UVGI system configuration. Consider two typical systems as shown in Figure 10a, which is commonly known as crossflow, and Figure 10b which is called axial flow. The kill zones developed from the above methodology, as implemented by the authors' software, are shown in Figure 11a and 11b for a single lamp system in a 57% reflective chamber and *Serratia marcescens* as the test microbe.

In Figure 11a, for the crossflow condition, the kill rate was predicted to be 59–64%, where 59% represents unmixed and 64% the mixed air conditions. In Figure 11b, using the same 5.5 watt lamp in the axial flow case, the range of kill rates was predicted to be 53–56%.

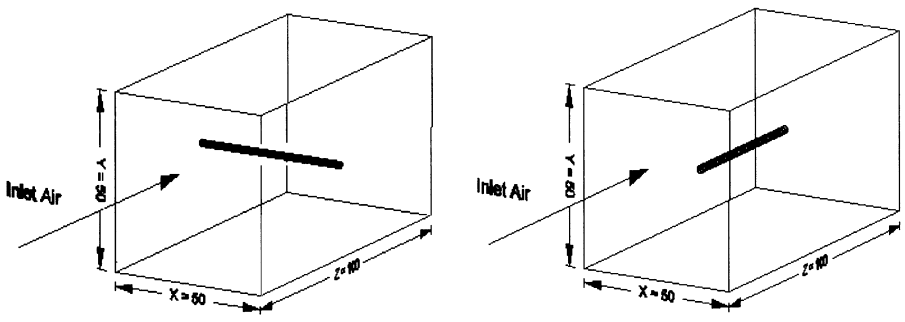

Figure l0a, b. Schematic of crossflow and axial flow configurations.

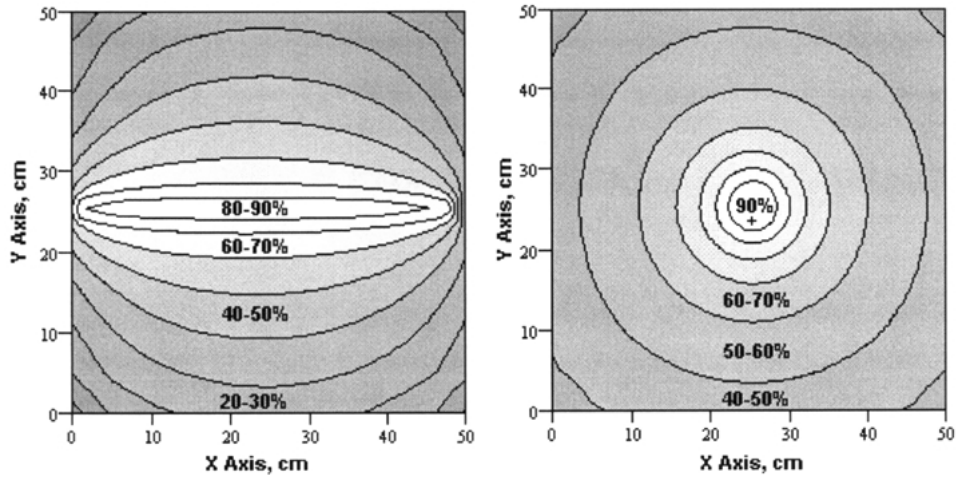

Figure 11a, b. Kill zones determined for the crossflow and axial test configurations, shown as percentage of population killed in unmixed air.

Table 4. Test parameters for *Bacillus subtilis* bioassays.

Parameter	Test #1	Test #2
Duct height, cm	30	30
Duct width, cm	64	64
Duct length, cm	91	91
Reflectivity, %	57.4	57.4
Lamp model	TUV36 PL-L	TUV36 PL-L
Lamp UV Watts (each)	24.0	24.0
# of lamps	2	1
Lamp configuration	crossflow	crossflow
Lamp arclength, cm	73	73
Lamp radius, cm	0.9	0.9
Airflow, m^3/s	0.9439	0.9439
Air velocity, m/s	4.877	4.877
Temperature, C	22	22
Relative humidity, %	45	45
Axerage intensity, $\mu W/cm^2$	6220	3939
Exposure time, sec	0.1875	0.1875
Dose received, $\mu J/cm^2$	1166	739
Standard rate constant, $cm^2/\mu J$	0.000449	0.000449
Air sampler	Andersen 6-stage	Andersen 6-stage
Upstream concentration, cfu/m^3	2000 (approx.)	2000 (approx.)
Downstream concentration, cfu/m^3	1200 (approx.)	1300 (approx.)
Standard deviation, $+/-\%$	4.7–8.6	4.7–8.6
Measured kill rate, %	37	31
Predicted mixed air kill rate, %	40.8	28.2
Predicted unmixed air kill rate, %	38.6	27.5

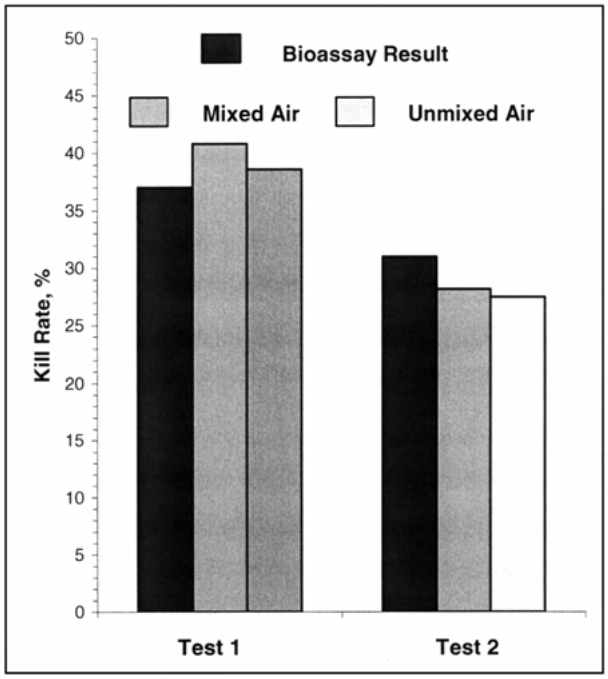

Figure 12. Bioassay results compared against the predictive model for *Bacillus subtilis*, for two systems, based on data from UVDI (2000).

The computer program developed by the authors can resolve the intensity field for any reflective rectangular enclosure, which can then be used to determine airborne rate constants from bioassays. This program has been used to interpret test data from over twenty laboratory tests to determine the airborne rate constant for *Serratia marcescens*, which has been found to be approximately $0.00291\,\mathrm{cm}^2/\mu\mathrm{J}$ (Kowalski and Bahnfleth, 2000).

The program has also determined the rate constant of *Bacillus subtilis*, to be approximately $0.000449\,\mathrm{cm}^2/\mu\mathrm{J}$, which closely corroborates the results of Sharp (1940). Data from airborne tests of *Bacillus subtilis* was provided from an independent source (UVDI, 2000b) and the data for this test is summarized in Table 4. A comparison of the laboratory results with model predictions is shown in Figure 12.

5. Relative Humidity Effects

Various sources state that increased relative humidity (RH) decreases the decay rate under UVGI exposure (Riley and Kaufman, 1972; Philips, 1985). Lidwell and Lowbury (1950) showed the rate constant for *Serratia marcescens* decreasing with increasing RH.

Rentschler and Nagy (1942) showed the rate constant for *Streptococcus pyogenes* increasing with increasing RH.

These results suggest that the relationship between RH and UVGI susceptibility is at least species-dependent and therefore no definitive general relationship can be established at present. Furthermore, no RH study can be performed without aerosolizing microorganisms and this requires more detailed treatment of the 3D intensity field than has previously been accomplished. Since RH impacts the measured rate constant, tests on the impact of RH are essentially measurements of the rate constant and can be given the same analytical treatment.

6. Sources of Predictive Error

Several sources may contribute errors to the predictions of the view factor model, including the error in the lamp wattage, variations in local voltage, errors in the photosensor readings, and variations of surface intensity along the lamp. The rate constant itself is subject to some level of microbiological uncertainty.

A comparison of predicted ratings using the view factor model for over 90 different UVGI lamp indicates predictive errors within ±9% (Kowalski and Bahnfleth, 2000). This assumes that the ratings are accurate, but there are likely to be inherent errors in the published ratings as well as the nominal UV power.

According to Severin and Roessler (1998) the largest error in the lamp photosensor is due to the setback of the sensor inside the body of the photosensor, or an error of 1 cm in the distance to the source. Additionally, readings cannot be taken at distances defined more accurately than about 0.1 cm. Finally, the photosensor itself has some inherent error.

The UV power output and lamp rating specified for UVGI lamps may vary. Manufacturers typically state the error in the nominal UV wattage is ±1% but this may be optimistic. Blatchley (1997) measured wattage variations in the same model lamp of +3.7%/−2.2%. These variations and uncertainties point out the need for improved methods of verifying lamp power.

Measurements should either be taken of all parameters that could affect the predictive accuracy of the model, including lamp wattage, line voltage, and the reflectivity of surfaces, or else the lamp intensity field itself should be corroborated with measurements.

7. Results and Discussion

A comprehensive mathematical model of UVGI disinfection has been presented which includes a new model for the shoulder portion of the survival curve. A model for the 3D intensity field of a UVGI system has been summarized that offers investigators the possibility of extracting rate constants from tests on aerosolized microorganisms.

Airborne rate constants have been determined or corroborated using these models for *Serratia marcescens* and *Bacillus subtilis*. Table 2 summarizes parameters for two stage decay curves and Table 3 summarizes shoulder parameters based on re-analysis of published test data.

The problem of air mixing in conjunction with the 3D intensity field has been addressed by establishing bounds or error limits within which investigators can determine UVGI rate constants in aerosol based studies.

The methods and equations presented here will enable microbiologists to accurately interpret aerosol studies on UVGI disinfection and to design better experiments. Since studies on relative humidity effects require the use of aerosols the methods presented here will facilitate the resolution of the humidity effects question. The authors have developed software for this purpose and can provide interpretation of experimental results for researchers conducting such experiments.

The authors hope that this information will stimulate new studies of UVGI disinfection, especially in relation to the determination of UVGI rate constants for all airborne pathogens and the study of relative humidity effects on rate constants. The resolution of the rate constants for all airborne pathogens will greatly assist the design of new, more effective systems for the control of airborne disease.

References

R.L. Abshire, H. Dunton, Applied and Environmental Microbiology **41**, 1419–1423 (1981).
A. Anellis, N. Grecz, D. Berkowitz, Applied Microbiology **13**, 397–401 (1965).
S.C. Antopol, P.D. Ellner, Applied and Environmental Microbiology **38**, 347–348 (1979).
A. Asthana, R.W. Tuveson, International Journal of Plant Science **153**, 442–452 (1992).
C.B. Beggs, K.G. Kerr, J.K. Donelly, P.A. Sleigh, D.D. Mara, G. Cairns, Transactions of the Royal Society of Tropical Medicine and Hygiene **94**, 141–146 (2000).
E.F. Blatchley, Water Research **31**, 2205–2218 (1997).
A.P. Casarett, *Radiation Biology* (Prentice-Hall, Englewood, 1968).
O. Cerf, Journal of Applied Bacteriology **42**, 1–19 (1977).
H. Chick, Journal of Hygiene **8**, 92 (1908).
F.M. Collins, Applied Microbiology **21**, 411–413 (1971).
H.L. David, The American Review of Respiratory Disease **108**, 1175–1184 (1973).
I.A. Davidovich, G.P. Kishchenko, Molecular Genetics, Microbiology and Virology **6**, 13–16 (1991).
W.B. Elmer, *The Optical Design of Reflectors* (TLA Lighting Consultants, Inc., Salem, MA, 1989).
H. Fujikawa, T. Itoh, Applied Microbiology **62**, 3745–3749 (1996).
G.J. Galasso, D.G. Sharp, Journal of Bacteriology **90**, 1138–1142 (1965).
F.L. Gates, Journal of General Physiology **13**, 231–260 (1929).
R.W. Gilpin, in *Legionella: Proceedings of the 2nd International Symposium*, edited by C. Thornsberry (American Society for Microbiology, Washington, 1984).
W. Harm, *Biological Effects of Ultraviolet Radiation* (Cambridge University Press, New York, 1980)
W.F. Hill, F.E. Hamblet, W.H. Benton, E.W. Akin, Applied Microbiology **19**, 805–812 (1970).
IES, *Lighting Handbook Application Volume* (Illumination Engineering Society, 1970).
S.M. Jacob, J.S. Dranoff, AIChE Journal **16**, 359–363 (1970).
M.M. Jensen, Applied Microbiology **12**, 418–420 (1964).
L.C. Keller, T.L. Thompson, R.B. Macy Applied and Environmental Microbiology **43**, 424–429 (1982).
G.B. Knudson, Applied and Environmental Microbiology **52**, 444–449 (1986).
A.L. Koch, *Bacterial Growth and Form* (Chapman & Hall, New York, 1995).
W.J. Kowalski, W.P. Bahnfleth, ASHRAE Transactions **106**, 4–15 (2000).
W.J. Kowalski, PhD Thesis, The Pennsylvania State University (2001).
O.M. Lidwell, E.J. Lowbury, Annual Review of Microbiology **14**, 38–43 (1950).
J.S. Little, R.A. Kishimoto, P.G. Canonico, Infection Immunity **27**, 837–841 (1980).

M. Luckiesh, *Applications of Germicidal, Erythemal and Infrared Energy* (D. Van Nostrand Co., New York, 1946).
E. Mitscherlich, E.H. Marth, *Microbial Survival in the Environment* (Springer-Verlag, Berlin, 1984).
W.A. Moats, R. Dabbah, V.M. Edwards, Journal of Food Science **36**, 523–526 (1971).
M.F. Modest, *Radiative Heat Transfer* (McGraw-Hill, New York, 1993).
J. Mongold, Genetics **132**, 893–898 (1992).
N. Munakata, M. Saito, K. Hieda, Photochemistry and Photobiology **54**, 761–768 (1991).
Philips, *Germicidal Lamps and Applications* (Catalog No. U.D.C. 628.9, Netherlands, 1985).
K.M. Pruitt, D.N. Kamau, Journal of Industrial Microbiology **12**, 221–231 (1993).
R.G. Qualls, J.D. Johnson, Applied Microbiology **45**, 872–877 (1983).
R.O. Rahn, P. Xu, S.L. Miller. Photochemistry and Photobiology **70**, 314–318 (1999).
A.J. Rainbow, S. Mak, International Journal of Radiation Biology **24**, 59–72 (1973).
H.C. Rentschler, R. Nagy, G. Mouromseff, Journal of Bacteriology **42**, 745–774 (1941).
H.C. Rentschler, R. Nagy, Journal of Bacteriology **44**, 85–94 (1942).
R.L. Riley, M. Knight, G. Middlebrook, American Review of Respiratory Disease **113**, 413–418 (1976).
R.L. Riley, J.E. Kaufman, Applied Microbiology **23**, 1113–1120 (1972).
W.M. Rohsenow, J.P. Hartnett, *Handbook of Heat Transfer* (McGraw-Hill, New York, 1973).
A.D. Russell, *The Destruction of Bacterial Spores* (Academic Press, New York, 1982).
B.F. Severin, M.T. Suidan, R.S. Englebrecht, Water Research **17**, 1669–1678 (1983).
B.F. Severin, M.T. Suidan, B.E. Rittmann, R.S. Englebrecht, Journal of Water Pollution Control **56**, 164–169 (1984).
B.F. Severin, P.F. Roessler, Water Research **32**, 1718–1724 (1998).
G. Sharp, Journal of Bacteriology **37**, 447–459 (1939).
G. Sharp, Journal of Bacteriology **38**, 535–547 (1940).
G.H. Smerage, A.A. Teixeira, Journal of Industrial Microbiology **12**, 211–220 (1993).
M.T. Suidan, B.F. Severin, AIChE Journal **32**, 1902–1909 (1986).
UVDI, Report on Bioassays of *S. marscecens* and *B. subtilis* exposed to UV irradiation. Ultraviolet Devices, Inc. (2000).
Y. Wang, A. Casadevall, Applied Microbiology **60**, 3864–3866 (1994).

ERRATA for

Mathematical Modeling of Ultraviolet Germicidal Irradiation for Air Disinfection

On page 263 in equation (19), the second ATAN function should have a square root in the denominator as follows:

$$F_h = \frac{1}{2p}\left[\begin{array}{l} \dfrac{X}{\sqrt{1+X^2}}\,ATAN\left(\dfrac{Y}{\sqrt{1+X^2}}\right) \\ +\dfrac{Y}{\sqrt{1+Y^2}}\,ATAN\left(\dfrac{X}{\sqrt{1+Y^2}}\right) \end{array}\right] \qquad (19)$$